AVO inversion for a non-welded interface
Estimating compliances of a fluid-filled fracture

Minato, Shohei; Ghose, Ranajit

DOI
10.1093/gji/ggw138

Publication date
2016

Document Version
Final published version

Published in
Geophysical Journal International

Geophysical Journal International

Geophys. J. Int. (2016) **206,** 56–62
Advance Access publication 2016 April 15
GJI Seismology

doi: 10.1093/gji/ggw138

AVO inversion for a non-welded interface: estimating compliances of a fluid-filled fracture

Shohei Minato and Ranajit Ghose

Department of Geoscience and Engineering, Delft University of Technology, 2628 CN Delft, The Netherlands. E-mail: s.minato-1@tudelft.nl

Accepted 2016 April 6. Received 2016 April 4; in original form 2015 December 4

SUMMARY

Though well known for layer boundaries, the use of amplitude-versus-offset (AVO) variations for non-welded boundaries like fractures is not yet investigated. Depending on the seismic wavelength used, fractures can be regarded as thin, compliant zones in rocks, in different scales. We explore the potential of multiangle AVO inversion of *P-P* and *P-S* reflections from a fracture to estimate fracture properties. We conduct laboratory experiments to measure reflection responses of dry and wet fractures. The observed *P-P* reflections of the wet fracture and the fracture aperture are very well predicted by the non-welded interface model. We invert the angle-dependent *P-P* reflectivity of the fracture to estimate both normal and tangential fracture compliances. The estimated value of the normal compliance is accurate, and it is also possible to obtain the value of the non-zero tangential compliance. We find that supplementing the information of converted *P-S* reflections in the AVO inversion greatly improves the estimate of the tangential compliance. The calculated compliance ratio clearly shows the existence of fluid in the fracture. This finding can be crucial for new applications in a wide range of scale—from earthquake seismology, deep and shallow seismic exploration, to non-destructive material testing.

Key words: Inverse theory; Defects; Fracture and flow; Body waves; Fractures and faults.

1 INTRODUCTION

A non-welded interface is a boundary across which traction is continuous but seismic displacement is discontinuous (e.g. Schoenberg 1980). The model is found to be useful to represent a thin, compliant zone in materials, for example, fractures in rocks (Nagy 1992). In this study, we consider a plane-wave reflection problem of a non-welded interface: we consider elastic waves which have a wavelength that is larger than the thickness of a fracture and also larger than the spacing between the asperities of contact, but shorter than the lateral extent of the fracture (Gu *et al.* 1996; Pyrak-Nolte & Morris 2000). Depending on the seismic wavelength used, fractures can be regarded as various thin, compliant zones in rocks, in different scales. For example, in laboratory-scale experiments, reflection and transmission coefficients are used to characterize the compliances of natural fractures (e.g. Pyrak-Nolte *et al.* 1990; Lubbe *et al.* 2008) and to monitor the frictional strength of rough solid surfaces (Nagata *et al.* 2008). In field-scale seismic measurements, the concept of reflection/transmission response from a non-welded interface is useful to study large fractures, such as rock joints (e.g. Cook 1992; Li *et al.* 2014). The concept is also applicable to macroscopic faults: Worthington & Hudson (2000) discussed the use of non-welded interfaces to predict VSP responses of geological faults and Kame *et al.* (2014) discussed the feasibility of this concept to monitor earthquake cycle at a plate boundary.

The boundary condition of a non-welded interface can be written as,

$$\Delta \mathbf{u} = \mathbf{Z}\mathbf{t}, \tag{1}$$

where $\Delta\mathbf{u}$ and $\mathbf{t}$ are, respectively, the jump in the seismic displacement vector across the fracture interface and the traction vector in the fracture-oriented Cartesian coordinate. The fracture compliance matrix $\mathbf{Z}$ consists of normal (η_N) and tangential (η_T) compliances as $\mathbf{Z} = \mathrm{diag}(\eta_T, \eta_T, \eta_N)$. Note that this is a rotationally invariant compliance matrix (Schoenberg 1980) which is applicable mostly to small fractures. For joints or faults which may have asperity patterns with preferred orientation, one would expect different tangential fracture compliances in the two principal directions. The fracture compliances are related to the confining stress and the fluid flow properties (e.g. Hopkins *et al.* 1987; Pyrak-Nolte & Morris 2000). Furthermore, assuming a model with randomly distributed asperities and an effective aperture, η_N and η_T are found to be functions of the properties of the fracture (Worthington & Lubbe 2007):

$$\eta_N^{-1} = r^w \frac{4\mu}{\pi a}\left(1 - \frac{V_S^2}{V_P^2}\right)\left(1 + \frac{2\,(r^w)^{1/2}}{\sqrt{\pi}}\right) + \frac{\lambda' + 2\mu'}{\Delta}, \tag{2}$$

$$\eta_T^{-1} = r^w \frac{8\mu}{\pi a}\left(1-\frac{V_S^2}{V_P^2}\right)\left(1+\frac{2(r^w)^{1/2}}{\sqrt{\pi}}\right)\Big/\left(3-\frac{2V_S^2}{V_P^2}\right)+\frac{\mu'}{\Delta}, \tag{3}$$

where V_P, V_S and μ are, respectively, *P*-wave velocity, *S*-wave velocity and the shear modulus of the host material (rock without fracture), a is the mean radius of the contact areas (asperities), r^w is the proportion of the fracture surface area that is in contact, μ' and λ' are the Lamé constants of the fracture infill and Δ is the mean aperture of the fracture. Eqs (2) and (3) indicate that estimating the fracture compliances is useful for further constraints on asperity distribution, fracture aperture and infill materials.

The theoretical derivation of plane-wave reflection and transmission coefficients at a non-welded interface for arbitrary incidence angles is widely available (e.g. Schoenberg 1980; Gu *et al.* 1996; Chaisri & Krebes 2000). In the Supporting Information (Appendix A), we showed the theoretical *P-P* and *P-S* reflection coefficients of a non-welded interface within a homogeneous medium. The reflection coefficients at non-welded interfaces are complicated functions of incidence angle and frequency (eqs A.1 and A.2 in the Supporting Information). Although amplitude-versus-offset (AVO) variation at a layer boundary (i.e. a single welded interface) has been extensively used to estimate contrasting local properties (e.g. Shuey 1985; Rutherford & Williams 1989), the AVO response of a non-welded interface has not been utilized so far to estimate fracture compliances. This is mainly because of the lack of high-frequency components in the conventional exploration-scale seismic experiments, which cannot resolve sufficiently the reflections from a single fracture. However, recent developments in microseismic observation using boreholes have enabled successful field measurement of relatively high-frequency reflections from a single fracture (Reshetnikov *et al.* 2010). The majority of the earlier laboratory-scale fracture experiments has considered only normally incident seismic waves (e.g. Pyrak-Nolte *et al.* 1990; Lubbe *et al.* 2008) and a few earlier studies that have considered oblique incidence at a non-welded interface are especially for non-destructive material testing (e.g. Margetan *et al.* 1988; Liaptsis *et al.* 2006; Nam *et al.* 2012), where multiple incidence angles at a given point on the interface were not utilized in the inversion.

In this study, we consider *P-P* and *P-S* AVO variations at a non-welded interface owing to their important advantages over normal-incident reflections. First, considering oblique incidence is more realistic for *in situ* measurements where subsurface fractures are not aligned parallel to the survey line. Second, the use of the multiple oblique-incidence waves offers a new possibility for simultaneous and robust estimation of both η_N and η_T. Estimating the compliance ratio is especially useful for predicting the existence of fluid in the fracture (e.g. Bakulin *et al.* 2000; Lubbe *et al.* 2008). This estimation using only a *P*-wave source was not possible before. Finally, an obliquely incident *P* wave also produces the converted *P-S* wave at the non-welded interface. The *P-S* reflection coefficient is sensitive to η_T (Chaisri & Krebes 2000), thus promising to provide an estimate of η_T. The ability to predict the presence/absence and the nature of fluid at a buried non-welded boundary from the AVO response of elastic waves measured at the surface can be of great importance in earthquake seismology (e.g. in delineating fluids at a subduction zone), exploration geophysics (both on the scale of oil and gas exploration and shallow engineering appraisal of fractured rocks) and non-destructive material testing.

We measured the *P-P* and *P-S* AVO responses from a fracture in the laboratory. At first, we calculated the reflection coefficient of a water-filled fracture using the dry fracture response as the reference. We then checked the efficacy of the non-welded interface representation of the angle-dependent reflection responses. Finally, we explored the possibility and accuracy of multiangle AVO inversion for η_N and η_T from the measured angle-dependent *P-P* and *P-S* reflection coefficients at the fracture.

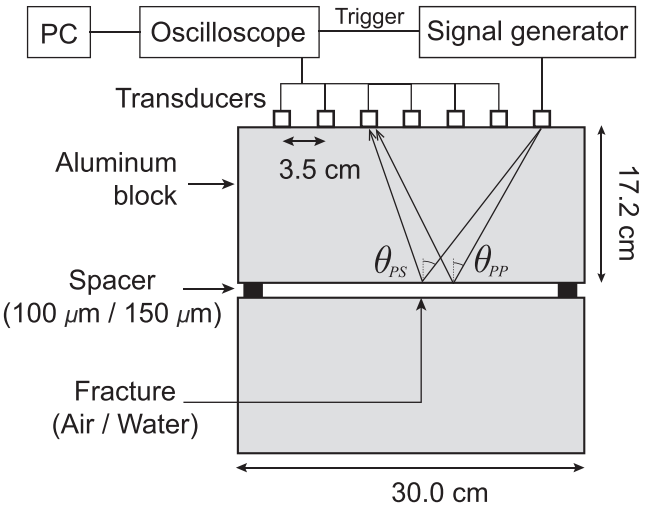

Figure 1. Experimental setup for measuring angle-dependent reflections from a fracture. Two incidence angles are illustrated: *P-P* reflection (θ_{PP}) and converted *P-S* reflection (θ_{PS}).

2 EXPERIMENT SETUP

Our experimental setup consists of two aluminum blocks with parallel and smooth surfaces (Fig. 1). From careful visual inspection and measurement of seismic velocity across the block in different directions, we assume that the aluminum block is homogeneous and isotropic (V_P = 6380 m s^{-1}, V_S = 3150 m s^{-1} and ρ = 2700 kg m^{-3}). An artificial horizontal fracture is simulated by installing spacers of known thicknesses (100 and 150 μm) between the two blocks. We installed seven longitudinal transducers (Panametrics V103) for an array-seismic measurement (one transmitter and six receivers). The spacing between the transducers is 3.5 cm: we obtain six incidence angles for both *P-P* reflections (5.8°, 11.5°, 17.0°, 22.1°, 27.0° and 31.4°) and *P-S* reflections (7.8°, 15.4°, 22.6°, 29.4°, 35.6° and 41.2°). We generated source signals (truncated sinusoid) with six different centre frequencies in the range 0.5–1.0 MHz.

We measured the reflection responses as follows. We assemble the two blocks with a spacer (100 or 150 μm) between them to simulate an air-filled (dry) fracture. After we measure the reflection responses of the dry fracture, we carefully lift the top block so that the receiver coupling does not change and we put a mixture of water and hair gel on the surface between the blocks. Then, we lower the top block to the original position in order to simulate a water-filled (wet) fracture and measure the reflection responses again.

Note that due to the spacers having a thickness larger than the surface roughness of the aluminum blocks (at most 38.1 μm), our fractures do not have surface asperities. In this case, the compliances can be represented as functions of the elasticity of the fracture-infill material and the fracture aperture (the second term in eqs 2 and 3). Furthermore, the fluid with a vanishingly small shear modulus results in a vanishingly small tangential stiffness of the fracture (second term in eq. 3). This is a situation when a fracture is modeled as a

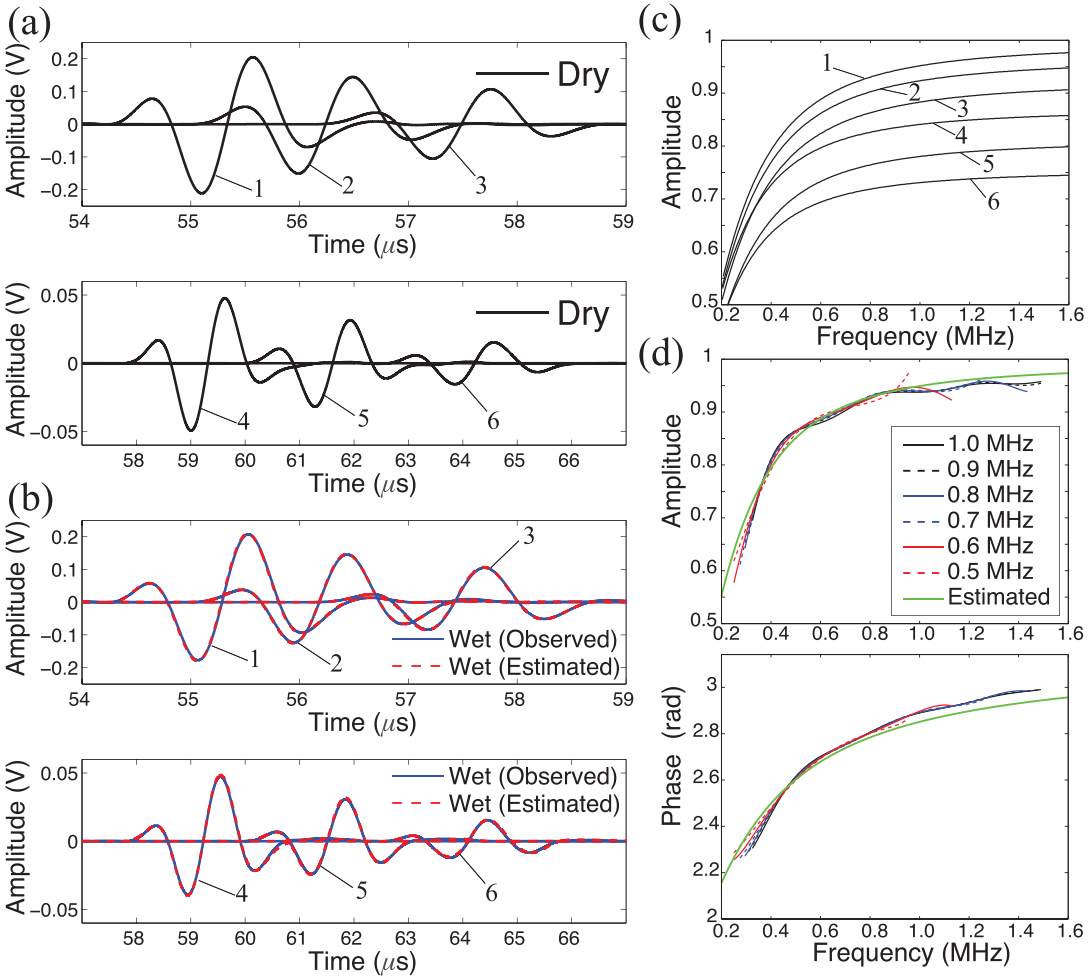

Figure 2. Observed angle-dependent *P-P* reflection responses for (a) dry fracture and (b) water-filled fracture. A 100-μm-thick spacer is used here. The numbered traces (1–6) refer to the six receivers. The wet-fracture response is estimated using the observed dry fracture response and the non-welded interface model. The estimated normal compliances are shown in Fig. 3. (c) The amplitude of the estimated *P-P* reflection coefficients of the wet fracture using the least-square inversion. The incident angles (θ_{PP}) are (1) 5.8°, (2) 11.5°, (3) 17.0°, (4) 22.1°, (5) 27.0° and (6) 31.4°. (d) Observed amplitude and phase spectra of the *P-P* reflection coefficients of the wet fracture ($\theta_{PP} = 5.8°$) derived from the source signal with the six different centre frequencies (0.5–1.0 MHz). The estimation from the inversion, using all data from different (centre frequency) source signals, are also shown.

thin, parallel-wall layer filled with a soft material which is often used to represent hydraulic fractures (e.g. Fehler 1982; Groenenboom & Fokkema 1998). In this vein, various earlier studies showed that a non-welded interface model approximates very well the reflection and transmission coefficients of a thin layer, provided the ratio of the thickness of the layer to the wavelength of radiation is small (e.g. Rokhlin & Wang 1991; Liu *et al.* 1995; Li *et al.* 2014). The wavelength of *P* waves in our experiment is approximately 6 mm or greater, which is larger than Δ (approximately 0.2 mm). Therefore, the wavelength of our experiment is suitable for representing the fracture as a non-welded interface.

3 EFFICACY OF THE NON-WELDED INTERFACE REPRESENTATION: ESTIMATION OF NORMAL COMPLIANCE FROM *P-P* AVO INVERSION

We checked the efficacy of the non-welded interface representation of angle-dependent reflection responses for the water-filled fracture by first estimating η_N at various incidence angles for the *P-P* reflections and then calculating the effective fracture aperture by assuming the tangential fracture stiffness (η_T^{-1}) to be zero.

3.1 Estimation of reflection coefficients of the wet fracture

We observed the *P-P* reflections for the dry and the wet fracture at the receiver array (six incidence angles) after bandpass (0.01–1.8 MHz) filtering and muting around the *P-P* reflections (Figs 2a and b). We used here 100-μm-thick spacer and 1.0 MHz centre frequency for the source signal. We assume that the difference between the dry and the wet fracture response is only in the reflection coefficients at the fracture and that the incident waves at the fracture and the effect of propagation (e.g. geometrical spreading and attenuation) between the source and receivers are identical between dry and wet conditions. Because the dry fracture responses are equivalent to the free-surface ones, the incident wave can be estimated from the dry fracture responses divided by the theoretical free-surface reflection coefficients (e.g. Aki & Richards 2002). The reflection coefficients of the wet fracture are then calculated by dividing in the frequency domain the observed wet fracture response (Fig. 2b)

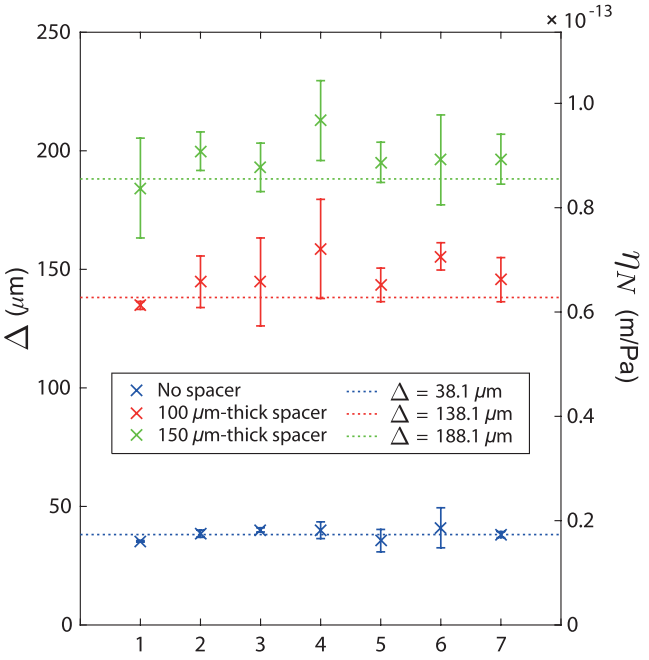

Figure 3. Estimated normal compliances (η_N) of the water-filled fracture without spacer and with 100- and 150-μm-thick spacer. The fracture aperture (Δ) is calculated from η_N (the second term of eq. 2) using the bulk modulus of water (2.2 GPa). The mean values and error bars are obtained from three-times independently repeated tests at each experiment. The horizontal axis presents the six incidence angles (θ_{PP}): (1) 5.8°, (2) 11.5°, (3) 17.0°, (4) 22.1°, (5) 27.0°, (6) 31.4° and (7) result from simultaneously inverting the observed reflection coefficients for all six incidence angles. The true apertures (red and green dotted lines) are obtained as the spacer thickness plus the residual aperture (38.1 μm), described in the text.

by the estimated incident waves. Thus, we calculate the angle- and frequency-dependent *P-P* reflection coefficient of the wet fracture ($R_{PP}^{\mathrm{Wet}}(\omega, \theta_{PP})$) using the following relation:

$$R_{PP}^{\mathrm{Wet}}(\omega, \theta_{PP}) = R_{PP}^{\mathrm{FS}}(\theta_{PP}) \frac{D^{\mathrm{Wet}}(\omega, \theta_{PP})}{D^{\mathrm{Dry}}(\omega, \theta_{PP})}, \tag{4}$$

where R_{PP}^{FS} is the theoretical free-surface *P-P* reflection coefficients (eq. A.7 in the Supporting Information). D^{Wet} and D^{Dry} are the reflection responses for the wet and the dry fracture, respectively. We assume that this procedure compensates for the source directivity, the changes in receiver coupling over the receiver array, and the propagation effect between the source and the receiver.

The observed reflection coefficients are coherent over all source signals with different centre frequencies (Fig. 2d). The reflection coefficient of the wet fracture is estimated using a least-square fitting of the observed coefficients with the theoretical *P-P* reflection coefficients for a non-welded interface (eq. A.1 in the Supporting Information) as a function of η_N. The estimated values of η_N at different incidence angles are summarized in Fig. 3. The estimated reflection coefficient clearly demonstrates the AVO effect for the non-welded interface (Fig. 2c). Finally, the predicted waveforms of the wet fracture using the estimated values of η_N match quite well with the observed angle-dependent reflection responses (red lines in Fig. 2b).

3.2 Evaluation of the estimated normal compliance

Using the value of the bulk modulus of water (2.2 GPa), we estimated the effective aperture of the fluid-filled fracture from η_N, using the second term of eq. (2). Here, we repeated the experiment three times independently, and showed the mean value and the standard deviation of the derived η_N and Δ in Fig. 3. In the Supporting Information, we discuss the details of the reproducibility test. The estimated apertures are larger than the installed spacer thickness (see red lines in Fig. 3) because a residual aperture is effectively created due to the dents and scratches on the surface of the aluminum blocks. To evaluate this residual aperture, we performed the same procedure described in the previous subsection again but without installing the spacer. We find that the average residual aperture is 38.1 μm over all receivers (blue dotted line in Fig. 3). Note that here we ignored the effect of surface asperities and assumed a thin, parallel-wall layer to estimate the residual aperture. From prior normal-incidence *SH*-wave measurements, we found that there was no significant shear energy transmitted across the fracture without the spacer, possibly due to the long-wavelength discrepancy from the planarity of the surface. Therefore, we assume that the asperities do not play an important role in this experiment, that is, we neglect the first term in eqs (2) and (3) even for the experiment with no spacer.

When we compare the estimated values of the fracture aperture with the true aperture values (i.e. spacer thickness + residual aperture), we find that the non-welded interface model estimates reasonably well the fracture aperture for all incidence angles (red lines in Fig. 3). We also performed the same experiment with 150-μm-thick spacer (green lines in Fig. 3). The results again confirm that the non-welded interface model estimates reasonably well the fracture aperture for all angles of incidence. Note that the estimated values of η_N tend to be larger than those we expect (green and red dotted lines in Fig. 3). Because the variation of the estimated η_N is mainly due to the amplitude variation of the water-filled fracture (see the Supporting Information), it could be due to the remaining bubbles at the fracture, which make the fracture more compliant.

4 NORMAL AND TANGENTIAL COMPLIANCE USING *P-P* AND *P-S* AVO INVERSION

In the previous section, we assume that we have prior information that the fracture does not have asperities with zero tangential fracture stiffness (η_T^{-1}). In this section, we assume that we do not have such prior information about the structure of the fracture and the material in the fracture. We then discuss the possibility of estimating simultaneously both η_N and η_T using *P-P* and *P-S* AVO responses.

Note that the true value of η_T is very large and cannot be resolved accurately in this experiment for the fracture scale and the frequency range that we use. This is because the reflection coefficients (see eqs A.1 and A.2 in the Supporting Information) are insensitive to the large values of η_T. However, the computed misfit of the observed reflection coefficients provides the possible lowest value of η_T, which is crucial information in order to infer the structure of the fracture. We further estimated compliance ratio (η_N/η_T) in order to discuss the existence of fluids in the fracture (e.g. Bakulin *et al.* 2000; Lubbe *et al.* 2008). The AVO inversion offers the possibility of estimating the compliance ratio without using a *S*-wave source, which was not possible before.

We assume here the fracture compliances to be spatially constant along the fracture plane. The approach can, however, handle heterogeneous fracture compliances through processing of each common-midpoint gathers. Recently, scattered elastic waves have been used

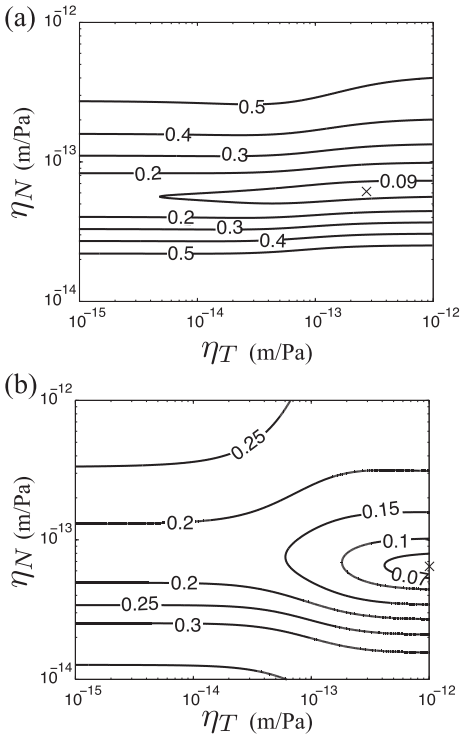

Figure 4. The normalized misfit function in (a) multiangle *P-P* AVO inversion and (b) joint *P-P* + *P-S* AVO inversion as a function of normal (η_N) and tangential (η_T) compliances.

to characterize heterogeneous fracture compliances (e.g. Leiderman *et al.* 2007; Minato & Ghose 2013, 2014).

4.1 *P-P* AVO inversion

We first consider only *P-P* reflections, when the spacer thickness is 100 μm (Fig. 2). We performed the same procedure as in the previous section to obtain the observed reflection coefficients (Fig. 2c). We then estimated η_N and η_T by minimizing the misfit between the observed and the estimated reflection coefficients for all incidence angles simultaneously. The normalized misfit function S is defined as,

$$S(\eta_N, \eta_T) = \frac{\sqrt{\sum_i \sum_j \left| R_{PP}^{\text{obs}}(\omega_i, \theta_j) - R_{PP}^{\text{est}}(\omega_i, \theta_j, \eta_N, \eta_T) \right|^2}}{\sqrt{\sum_i \sum_j \left| R_{PP}^{\text{obs}}(\omega_i, \theta_j) \right|^2}}, \quad (5)$$

where $R_{PP}^{\text{obs}}(\omega_i, \theta_j)$ and $R_{PP}^{\text{est}}(\omega_i, \theta_j)$ are, respectively, the observed and the estimated *P-P* reflection coefficients for the jth incident angle and the ith frequency component.

We calculated the misfit function considering the ranges of the compliances to be $10^{-14} \leq \eta_N \leq 10^{-12}$ and $10^{-15} \leq \eta_T \leq 10^{-12}$. We discretized the compliance ranges in 400 × 400 samples and calculated the contour map of the normalized misfit function (Fig. 4a). Note that we considered the upper bound of η_T to be 10^{-12} m Pa^{-1} because in the given frequency range we hardly see any changes in the theoretical *P-P* reflection coefficients and in the corresponding $S(\eta_N, \eta_T)$ for values of η_T larger than 10^{-12} m Pa^{-1}. The misfit function shows that η_N is more sensitive than η_T (Fig. 4a). Furthermore, it illustrates that the estimated η_T is of the same order of magnitude or larger than η_N (see contour of 0.09 in Fig. 4a). The estimated minimum misfit in the inversion is located at $(\eta_N, \eta_T) = (6.12 \times 10^{-14}, 1.51 \times 10^{-13})$. Therefore, we obtain an accurate estimate of η_N (see Fig. 3 for the true value). Due to the small sensitivity of η_T to the *P-P* reflection coefficient, however, the compliance ratio η_N/η_T (a fluid indicator) is detected as 0.40. Unfortunately, this value of compliance ratio is too large for a wet natural fracture created in a laboratory experiment (Lubbe *et al.* 2008), which implies that this can be misinterpreted as a dry natural fracture. Nevertheless, Fig. 4(a) shows that we can detect the possible lowest value of non-zero η_T from multiangle *P-P* AVO inversion. In our experiment, we have a maximum incidence angle of 31.4°. The use of higher incidence angles will improve the sensitivity to η_T, as shown in Chaisri & Krebes (2000).

4.2 Joint inversion using *P-P* and *P-S* AVO responses

We introduced the *P-S* reflections in the inversion procedure described in the previous subsection. The similar procedure was applied to calculate the *P-S* reflection coefficients (eq. A.2 in the Supporting Information) for the wet fracture. The calculated *P-P* and *P-S* reflection coefficients were then simultaneously inverted to estimate η_N and η_T.

The calculated contour map of the misfit function (Fig. 4b) shows that the sensitivity to η_T is now greatly improved from the one using only *P-P* reflections (Fig. 4a). The estimated minimum misfit is located at $(\eta_N, \eta_T) = (6.49 \times 10^{-14}, 1.00 \times 10^{-12})$. Note that η_T is estimated to be at the upper bound of the range: η_T is found to be at least two orders of magnitude larger than η_N. The resulting compliance ratio is shown to be 0.0649, which can be clearly interpreted as a wet fracture (Lubbe *et al.* 2008). The predicted *P-S* reflection waveforms using the estimated values of η_N and η_T match quite well with the observed angle-dependent *P-S* reflection responses (Fig. 5).

Note that although our situation is not same as that of a natural fracture containing asperities, the estimated values of η_N are similar to those of natural fractures (Lubbe *et al.* 2008). Furthermore, because of the large value of η_T, we obtain the possible lowest value for η_T. However, laboratory experiments using natural fractures show that η_T of a dry/wet fracture is of the same order of magnitude as η_N (Lubbe *et al.* 2008). Therefore, we expect to obtain more accurate values of η_T for natural fractures using the AVO inversion developed in this study, although it requires additional laboratory verification.

5 CONCLUSIONS

We conducted ultrasonic laboratory experiments to measure *P-P* and *P-S* AVO responses from a non-welded interface (a dry and wet fracture) using aluminum blocks and spacers with known thicknesses (100 and 150 μm). We estimated the reflection response of the wet fracture using the dry fracture response as a reference. By estimating the normal compliance and corresponding fracture aperture, we confirmed that the non-welded interface model for a fluid-filled fracture describes quite well the angle-dependent *P-P* reflection responses, which indicates that the measurement using a long seismic wavelength (approximately 6 mm) correctly handles the reflections from a very thin (approximately 0.2 mm) layer.

Furthermore, we found that both normal and tangential compliances can be estimated from the multiangle *P-P* AVO inversion. Our results showed that the normal compliance can accurately be obtained and that it is possible to estimate also the non-zero tangential compliance. Finally, we found that a joint inversion of *P-P* and *P-S* AVO responses greatly improves the estimation of the tangential compliance. We used only six traces (six angles of incidence) for

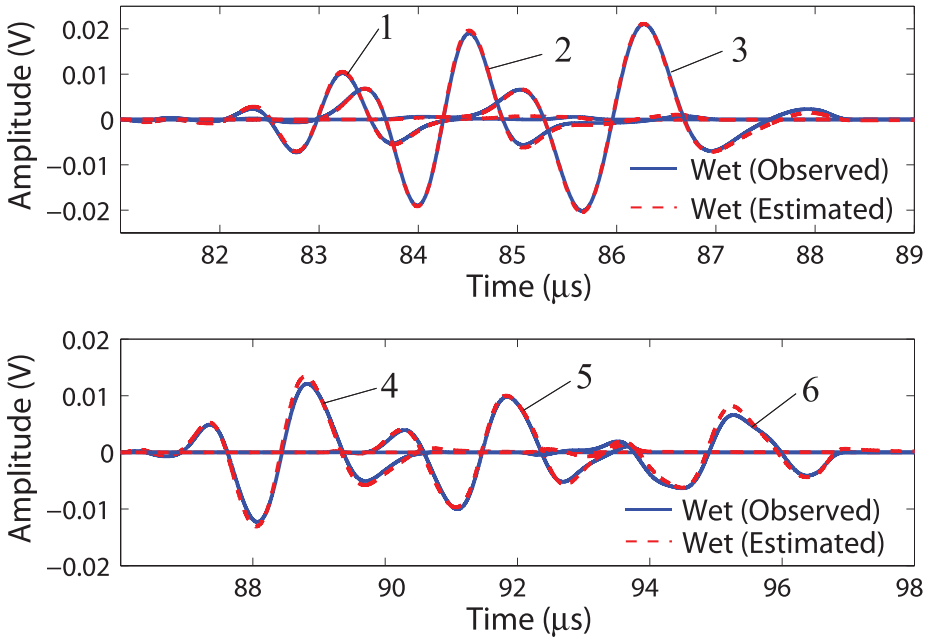

Figure 5. Observed and estimated angle-dependent *P-S* reflection responses of the water-filled fracture with a 100-μm-thick spacer. The estimated responses are derived using the non-welded interface model and joint *P-P* + *P-S* AVO inversion, described in the text. The incident angles (θ_{PS}) are (1) 7.8°, (2) 15.4°, (3) 22.6°, (4) 29.4°, (5) 35.6° and (6) 41.2°.

the AVO inversion of the laboratory experimental data. However, in real-field applications involving multiple sources and receivers, the number of traces and the range of incidence angle available for AVO inversion will be much greater, which would result in more robust estimates of fracture compliances in the presence of noise. The derived normal to tangential compliance ratio clearly showed the existence of fluid in the fracture, a finding that has a major application potential in wide ranges of scale and discipline.

ACKNOWLEDGEMENTS

We thank Leon Thomsen and an anonymous reviewer for their helpful reviews and constructive comments that significantly improved the manuscript. We thank Karel Heller for his assistances in laboratory experiments. This work is supported by The Netherlands Research Centre for Integrated Solid Earth Science (ISES).

REFERENCES

Aki, K. & Richards, P.G., 2002. *Quantitative Seismology,* 2nd edn, University Science Books.

Bakulin, A., Grechka, V. & Tsvankin, I., 2000. Estimation of fracture parameters from reflection seismic data–Part I: HTI model due to a single fracture set, *Geophysics,* **65**(6), 1788–1802.

Chaisri, S. & Krebes, E.S., 2000. Exact and approximate formulas for P-SV reflection and transmission coefficients for a nonwelded contact interface, *J. geophys. Res.,* **105**(B12), 28 045–28 054.

Cook, N., 1992. Natural joints in rock: mechanical, hydraulic and seismic behaviour and properties under normal stress, *Int. J. Rock Mech. Min. Sci. Geomech. Abstr.,* **29**(3), 198–223.

Fehler, M., 1982. Interaction of seismic waves with a viscous liquid layer, *Bull. seism. Soc. Am.,* **72**(1), 55–72.

Groenenboom, J. & Fokkema, J.T., 1998. Monitoring the width of hydraulic fractures with acoustic waves, *Geophysics,* **63**(1), 139–148.

Gu, B., Suárez-Rivera, R., Nihei, K.T. & Myer, L.R., 1996. Incidence of plane waves upon a fracture, *J. geophys. Res.,* **101**(B11), 25 337–25 346.

Hopkins, D.L., Cook, N.G. & Myer, L.R., 1987. Fracture stiffness and aperture as a function of applied stress and contact geometry, in *The 28th US Symposium on Rock Mechanics (USRMS),* pp. 673–680, American Rock Mechanics Association.

Kame, N., Nagata, K., Nakatani, M. & Kusakabe, T., 2014. Feasibility of acoustic monitoring of strength drop precursory to earthquake occurrence, *Earth Planets Space,* **66**(1), 1–12.

Leiderman, R., Barbone, P.E. & Braga, A.M.B., 2007. Reconstructing the adhesion stiffness distribution in a laminated elastic plate: exact and approximate inverse scattering solutions, *J. acoust. Soc. Am.,* **122**(4), 1906–1916.

Li, J., Li, H., Jiao, Y., Liu, Y., Xia, X. & Yu, C., 2014. Analysis for oblique wave propagation across filled joints based on thin-layer interface model, *J. appl. Geophys.,* **102,** 39–46.

Liaptsis, D., Drinkwater, B. & Thomas, R., 2006. The interaction of oblique incidence ultrasound with rough, partially contacting interfaces, *Nondestruct. Test. Eval.,* **21**(3–4), 109–121.

Liu, E., Hudson, J., Crampin, S., Rizer, W. & Queen, J., 1995. Seismic properties of a general fracture, in *Mechanics of Jointed and Faulted Rock,* pp. 673–678, A.A. Balkema Publishers.

Lubbe, R., Sothcott, J., Worthington, M. & McCann, C., 2008. Laboratory estimates of normal and shear fracture compliance, *Geophys. Prospect.,* **56**(2), 239–247.

Margetan, F., Thompson, R. & Gray, T., 1988. Interfacial spring model for ultrasonic interactions with imperfect interfaces: theory of oblique incidence and application to diffusion-bonded butt joints, *J. Nondestruct. Eval.,* **7**(3–4), 131–152.

Minato, S. & Ghose, R., 2013. Inverse scattering solution for the spatially heterogeneous compliance of a single fracture, *Geophys. J. Int.,* **195**(3), 1878–1891.

Minato, S. & Ghose, R., 2014. Imaging and characterization of a subhorizontal non-welded interface from point source elastic scattering response, *Geophys. J. Int.,* **197**(2), 1090–1095.

Nagata, K., Nakatani, M. & Yoshida, S., 2008. Monitoring frictional strength with acoustic wave transmission, *Geophys. Res. Lett.,* **35**(6), L06310, doi:10.1029/2007GL033146.

Nagy, P., 1992. Ultrasonic classification of imperfect interfaces, *J. Nondestruct. Eval.,* **11**(3–4), 127–139.

Nam, T., Lee, T., Kim, C., Jhang, K.-Y. & Kim, N., 2012. Harmonic generation of an obliquely incident ultrasonic wave in solid–solid contact interfaces, *Ultrasonics,* **52**(6), 778–783.

Pyrak-Nolte, L. & Morris, J., 2000. Single fractures under normal stress: The relation between fracture specific stiffness and fluid flow, *Int. J. Rock Mech. Min. Sci.,* **37,** 245–262.

Pyrak-Nolte, L., Myer, L. & Cook, N., 1990. Transmission of seismic waves across single natural fractures, *J. geophys. Res.,* **95**(B6), 8617–8638.

Reshetnikov, A., Buske, S. & Shapiro, S., 2010. Seismic imaging using microseismic events: results from the San Andreas fault system at SAFOD, *J. geophys. Res.,* **115,** B12324, doi:10.1029/2009JB007049.

Rokhlin, S.I. & Wang, Y.J., 1991. Analysis of boundary conditions for elastic wave interaction with an interface between two solids, *J. acoust. Soc. Am.,* **89**(2), 503–515.

Rutherford, S.R. & Williams, R.H., 1989. Amplitude-versus-offset variations in gas sands, *Geophysics,* **54**(6), 680–688.

Schoenberg, M., 1980. Elastic wave behavior across linear slip interfaces, *J. acoust. Soc. Am.,* **68**(5), 1516–1521.

Shuey, R., 1985. A simplification of the Zoeppritz equations, *Geophysics,* **50**(4), 609–614.

Worthington, M. & Lubbe, R., 2007. The scaling of fracture compliance, *Geol. Soc. Lond. Spec. Publ.,* **270**(1), 73–82.

Worthington, M.H. & Hudson, J.A., 2000. Fault properties from seismic Q, *Geophys. J. Int.,* **143**(3), 937–944.

SUPPORTING INFORMATION

Additional Supporting Information may be found in the online version of this paper:

Appendix A. Theoretical Reflection Coefficients.
Appendix B. Reproducibility Test.
Figure B1. Observed reflected waves at 6 different incidence angles at the dry fracture with a 100 μm-thick spacer. The source signal with 1.0 MHz centre frequency is used. Three lines (1, 2 and 3) in different colours indicate the record of three independent experiments.
Figure B2. Observed reflected waves at 6 different incidence angles at the water-filled fracture with a 100 μm-thick spacer. The source signal with 1.0 MHz centre frequency is used. Three lines (1, 2 and 3) in different colours indicate the record of three independent experiments.
(http://gji.oxfordjournals.org/lookup/suppl/doi:10.1093/gji/ggw138/-/DC1).

Please note: Oxford University Press is not responsible for the content or functionality of any supporting materials supplied by the authors. Any queries (other than missing material) should be directed to the corresponding author for the paper.